ACS OMEGA

http://pubs.acs.org/journal/acsodf

Article

Substrate for Surface-Enhanced Raman Spectroscopy Formed by Gold Nanoparticles Buried in Poly(methyl methacrylate)

Natalia K. Gushiken, Giordano T. Paganoto, Marcia L. A. Temperini, Fernanda S. Teixeira, and Maria Cecilia Salvadori*

Cite This: *ACS Omega* 2020, 5, 10366−10373

Read Online

ACCESS | Metrics & More | Article Recommendations

ABSTRACT: In this work, we present some properties and use of a nanocomposite formed by gold nanoparticles (NPs) into poly(methyl methacrylate) (PMMA) and its application as substrates for surface-enhanced Raman spectroscopy (SERS). The nanocomposite was formed using low-energy (49 eV) ion implantation of gold in PMMA using a cathodic arc plasma gun. The gold NPs are formed spontaneously from the implanted ions and they remain isolated from each other by the polymer medium surrounding them, ensuring a spacing between the NPs of less than 10 nm (hot spot places). The NPs form below the surface, protected from the environment, guaranteeing the stability of the composite layer. Moreover, here, we present an interesting approach to concentrate analyte molecules closer to the metal surface using the swelling effect in PMMA. Using absorption of the analyte, the molecules stay in the gaps between NPs, which is a good solution for one of the biggest challenges in SERS, that is, to guide molecules to the hot spot places.

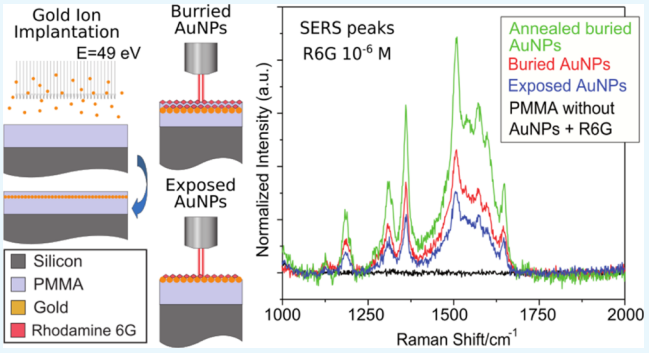

INTRODUCTION

Metallic nanoparticles (NPs) exhibit different optical and electrical properties than their bulk material; thus, there is great interest on the study of these nanoparticulate materials because of their applications in optics, sensing, biomedicine, biosensing, and plasmonics, among others.[1−3] In this context, one of the main challenges in chemical and biological sensing leading is the detection of traces of a given substance (analyte) and reaching the detection regime of a single molecule. One approach to detect small amounts of analytes is surface-enhanced Raman spectroscopy (SERS) and it could include single molecule detection and also provide information about the molecular structure of the sample.[4] For successful SERS analysis, it is important to have tailored substrates formed by metallic NPs distributed on a surface where the material to be analyzed is deposited.[5−7]

Since the first SERS demonstration on a silver electrode in 1975,[8] considerable efforts have been made to obtain effective SERS substrates.[9,10] Various substrates based on noble metals, such as Au, Ag, and Cu, exhibit superior SERS ability for localized surface plasmon resonance (LSPR), creating hot spots, which is considered as the dominant means to achieve the effect of SERS.[8,9,11] In the recent literature, great efforts have been made for the fabrication of effective SERS substrates based on noble metals, metallic oxides (ZnO, SnO_2, TiO_2, and others), two-dimensional materials (graphene, graphene oxide, and other derivatives and MoS_2),[8−12] and also metal−organic frameworks.[13] Among the noble metals cited above, the LSPR experiments have been carried out majorly with gold and silver NPs. Although silver and gold have similar refractive indexes, gold is commonly chosen because of its relative chemical inertness and resistance to oxidation.[3,8]

From a technology point of view, several efforts are made to produce effective SERS substrates, which overcome challenges such as high cost, time-consuming preparation, reproducibility, and stability.[10,11] Among the several methods[1,10,12,14−18] to synthesize gold NPs for SERS substrates, one of the main ways is to reduce a solvated gold salt in the presence of a surface-capping agent, which produces electrostatic repulsion between the particle, preventing aggregation.[19] However, many analyte molecules show low affinity toward the metal NPs; thus, one of the biggest challenges is to guide analyte molecules to the hot spot places.[13] Although several research studies[20−23] focus on functionalization of NPs to improve affinity of the analyte on the metal surface, the metallic colloid still easily aggregates.[24]

Received: January 10, 2020
Accepted: April 21, 2020
Published: April 30, 2020

To prevent aggregation, the most common approach is to coat metallic NPs with organic or inorganic shells,[25−28] but the diffusion of analyte molecules to the metal core is still limited. Thus, this work presents an interesting approach to obtain metallic NP stability and concentrated analyte molecules closer to the metal surface: the NPs are formed isolated from each other by the polymer medium, and the swelling effect in poly(methyl methacrylate) (PMMA) observed in this work concentrates the rhodamine 6G (R6G) molecules in the AuNP surroundings.

Low-energy (49 eV) ion implantation of gold in PMMA using cathodic arc plasma was used. The gold NPs are formed spontaneously, which can be explained by the occurrence of metal atom concentration above the solubility limit in the implanted substrate, leading to nucleation and formation of metallic NPs.[29] Through theoretical simulations, the literature reports[30] that the nucleation of gold NPs already occurs at an implantation dose of 1×10^{14} atoms/cm^2. Note that in this approach, the NPs are formed isolated from each other by the polymer medium surrounding them, ensuring a spacing between the NPs of less than 10 nm; additionally, NPs form below the surface, protected from the environment, guaranteeing the stability of the composite layer.

In summary, our main objective is to study the nanocomposite formed by gold NPs into PMMA and its application as substrates for SERS. The main techniques used for this study were SERS, transmission electron microscopy (TEM), ultraviolet−visible (UV−vis) spectrophotometry, and atomic force microscopy (AFM). Additionally, as complementation, SERS enhancement factor (EF) simulations using the generalized multiparticle Mie (GMM) method were used.

MATERIALS AND METHODS

PMMA Preparation. PMMA is an acrylic polymer, which is commonly used as a high-resolution positive e-beam resist. In order to obtain the composite material AuNP−PMMA investigated in this work, PMMA 950k A2 (2% PMMA, molecular weight of 950,000 g mol^{-1}) dissolved in anisole (from Microchem Corp.) was spin-coated onto a silicon substrate at 4000 rpm for 50 s to obtain an about 80 nm-thick PMMA film and then baked at 180 °C for 20 min to eliminate the casting solvent.

Gold Ion Implantation Setup. The ion implantation of gold was carried out inside a vacuum chamber (whose base pressure was about 10^{-6} Torr or 10^{-4} Pa) using cathodic arc plasma. With this technique, the final energy of gold ions reaching the sample is 49 eV,[31,32] which is enough for implanting gold ions to a depth of few nanometers below the PMMA surface.[33]

The gold ion implantation doses chosen for this work are based on prior results from Salvadori and coworkers,[34] in which some aspects of electrical conductivity of the system gold implanted in PMMA are described. According to these reported results, for having isolated gold NPs buried in the PMMA, the dose of gold implantation must be below 1×10^{16} atoms/cm^2 (percolation dose).

For this work, different doses were used for various experiments: 0.60×10^{16}, 0.64×10^{16}, 0.75×10^{16}, and 0.81×10^{16} atoms/cm^2; all of these were below the percolation dose, and the percolation dose was 1.02×10^{16} atoms/cm^2.

Experimental Determination of the Penetration Depth of Ion-Implanted Gold. The PMMA layer on the silicon substrate was e-beam-lithographed using a pattern of a matrix, consisting of 11 × 11 squares with dimensions of 5 × 5 μm^2 spaced by 10 μm. After the lithography process, the original PMMA film thickness h_0 was determined by measuring the structure steps (Figure 1b.1) by AFM in the intermittent contact mode. Following this, the gold ion implantation was performed on PMMA, generating the NP layer, and a new thickness measurement (h_1) was performed (Figure 1b.2) to verify the decrease in thickness due to the sputtering effect that occurs simultaneously with ion implantation. The difference between h_1 and h_0 gives information about polymer sputtering due to gold implantation.

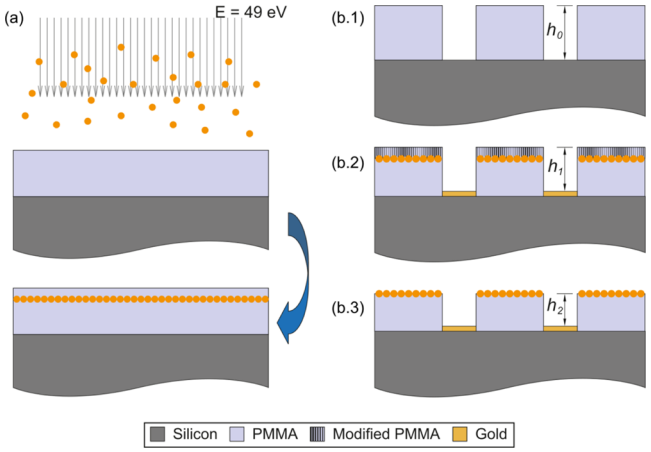

Figure 1. (a) Schematic of gold ion implantation in the PMMA thin film. (b) Schematic of measurements of (b.1) original PMMA film thickness, (b.2) that after ion implantation, and (b.3) that after the development of the PMMA layer above the NPs.

As the gold ion implantation energy (49 eV) was enough to break PMMA chains, the modified PMMA layer, on the top of the NP layer, was soluble in the developer solution (1 MIBK/3 IPA).[35] In this way, the PMMA on the top of the NP layer was removed, producing thickness h_2 (Figure 1b.3). The depth of the gold NPs inside the polymer is therefore the difference between h_1 and h_2.

SERS Instrumentation, Samples, and Analytes Used. Raman and SERS measurements were performed on a Renishaw InVia Raman microscope equipped with a He−Ne laser source at 632.8 nm, using a 50× objective lens (NA = 0.75), a diffraction grating of 1200 lines/mm, an accumulation time of 50 s, and a laser power of 0.36 mW/μm^2.

PMMA thin films with AuNPs and a PMMA thin film without gold (reference) were measured using SERS. The analyte 10 μM R6G ethanolic solution was applied over the surface of the AuNP−PMMA samples and also over the PMMA film reference sample. After 60 s, the spinner was run at 2000 rpm for 50 s. Then, the substrates were left to dry overnight in a desiccator with silica in vacuo at room temperature.

Atomic Force Microscopy. An atomic force microscope (Nanoscope IIIa, from Bruker Instruments, Santa Barbara) was used in the tapping mode to measure height steps and also surface roughness of some samples.

Samples for TEM. For top-view images, the sample preparation of the AuNP−PMMA for TEM was performed initially by cutting PMMA, with approximately 80 nm thickness, with a diamond knife by ultramicrotomy (Leica Ultramicrotome EM UC7, Germany). The cuts were placed in

https://dx.doi.org/10.1021/acsomega.0c00133
ACS Omega 2020, 5, 10366−10373

proper grids for the TEM technique and used as substrates for gold ion implantation using cathodic arc plasma. Together with the grids, a silicon control sample was used for further analysis of implanted doses by Rutherford backscattering spectrometry (RBS).

For a cross-sectional image, the sample preparation was performed by implanting Au in a bulk sample of PMMA with dimensions of about 2 mm.[3] After deposition, the sample was embedded into a Specifix-20 resin. Then, the sample was trimmed in a way to expose the cross-section of the composite layer, and by ultramicrotomy, cuts of about 80 nm thick were obtained.

GMM Simulations. GMM simulations for the SERS EF were done in order to have an insight about the effect of NPs' size and about the distance between them for SERS enhancement. This method uses an extension of Mie's theory for the case of multiple particles, being a semi-analytic solution for the scattering of light by an arbitrary set of isolated spheres.[36]

The excitation radiation for EF calculation was 633 nm, and the dielectric medium containing the particles was water in order to simplify the simulation (refractive index of the dielectric medium, n = 1.33). The geometric parameters used were based on the resulting NP geometry (NPs' average diameter and distance between NPs), as will be seen.

UV−Vis Instrumentation and Samples. The UV−vis spectra were obtained using a UV-3101PC UV-VIS-NIR spectrophotometer (from Shimadzu) in the transmission mode. The substrates consist of a thin film of PMMA over a glass substrate with AuNPs formed by gold ion implantation.

RESULTS AND DISCUSSION

Measurement of the AuNP Depth in PMMA and Exposure of NPs. As described above and shown in Figure 1, it was possible to measure the AuNP depth in PMMA. Thus, Figure 1b.1 represents the original thickness of the PMMA film designated as h_0. After an ion implantation dose of 1.02 × 10^{16} atoms/cm^2, new thickness measurement was performed, obtaining h_1 (Figure 1b.2). The difference between h_1 and h_0 (7 nm) indicates the PMMA decrease in thickness due to the sputtering effect that occurs simultaneously with the ion implantation. After that, the samples were developed and one more thickness measurement was performed (Figure 1b.3), obtaining h_2. The difference between h_1 and h_2 (10 nm) indicates the removal of the polymer layer above the AuNP−PMMA composite layer, that is, confirming that the energy of 49 eV of ion implantation was enough for breaking chains in the PMMA, making this layer soluble in the developer solution.

From this result, it can be inferred that AuNPs are formed in PMMA at a depth of about 10 nm. This result is confirmed by the cross-sectional TEM image presented in Figure 2a.

Another analyzed aspect was the effect of exposure of the AuNPs through the development of the PMMA layer above the composite layer after the ion implantation process. Top-view TEM images of the AuNP−PMMA before and after chemical development state that the NPs are not removed with the development. The development was performed directly in the grids after the ion implantation process using a dose of 0.75 × 10^{16} atoms/cm^2. Figure 2b shows a top-view image of AuNP−PMMA after the chemical development process.

Applying the Composite AuNP−PMMA as SERS Substrates. The analysis consisted of the study of the role of ion implantation doses on the intensity of the SERS

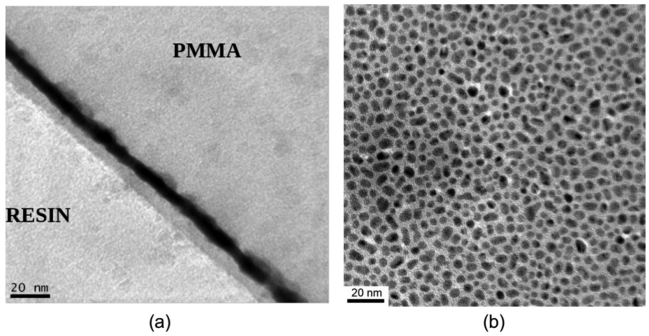

Figure 2. (a) Cross-sectional TEM image of AuNPs formed in PMMA by gold ion implantation with 49 eV and a dose of 1.0 × 10^{16} atoms/cm^2. (b) Top-view image from AuNP−PMMA after the chemical development process, for an implantation dose of 0.75 × 10^{16} atoms/cm^2.

spectrum. Thus, three spectra of R6G were obtained for different doses: 0.64 × 10^{16}, 0.81 × 10^{16} ,and 1.02 × 10^{16} atoms/cm^2 (percolation dose). Figure 3 presents SERS spectra using these three substrates, where the characteristic peaks of R6G are present. The band near 1000 cm^{-1} in all spectra is related to the multiphonon scattering generated by the silicon substrate under the PMMA thin film.[37] The effect of the increase of the gold implantation dose was an increase in the intensity of the bands. Figure 3b shows the intensity of the

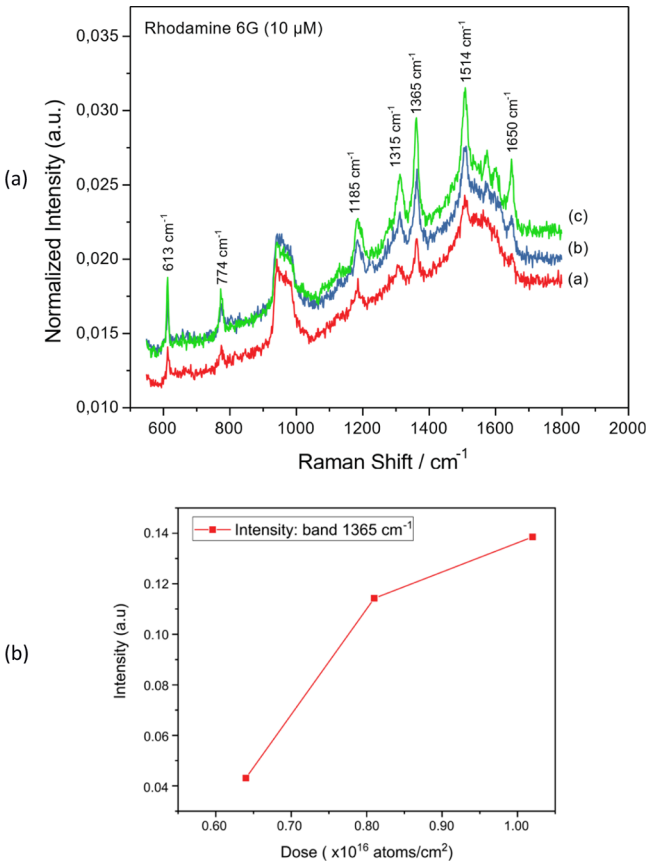

Figure 3. (a) SERS spectra of R6G on AuNP−PMMA obtained for different doses of ion implantation: 0.64 × 10^{16} atoms/cm^2 (red), 0.81 × 10^{16} atoms/cm^2 (blue), and 1.02 × 10^{16} atoms/cm^2 (green). No baseline correction was applied. (b) Intensity of the band at 1368 cm^{-1} vs the doses of ion implantation.

https://dx.doi.org/10.1021/acsomega.0c00133
ACS Omega 2020, 5, 10366−10373

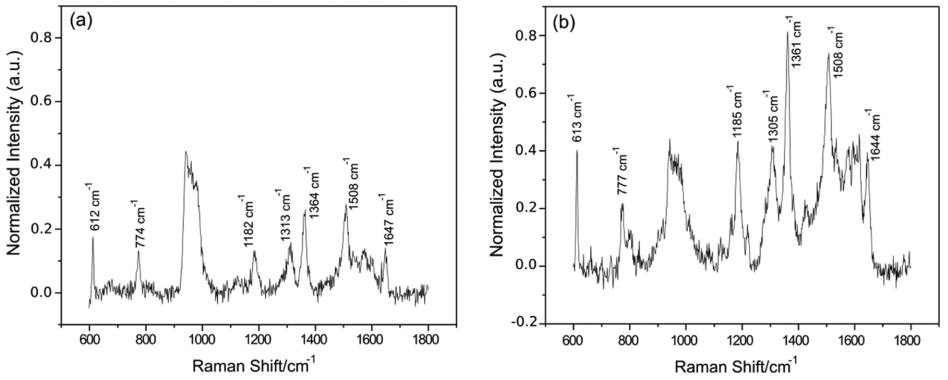

Figure 4. SERS from R6G (a) using a substrate with exposed AuNPs and (b) that with buried AuNPs into PMMA. A baseline correction was applied.

1365 cm^{-1} band as a function of the dose, which shows this trend clearly. This result is compatible with the fact that the distance between particles (nanogap) decreases as the implantation dose increases, leading to the percolation process, and it is known that lower the gap between particles, higher the SERS effect.

Thus, one of two substrates of AuNP−PMMA, with doses of 0.6×10^{16} atoms/cm^2, was developed, exposing the AuNPs. After that, the analyte R6G at 10 μM in ethanol was spin-coated over the surface of the substrate. Figure 4a presents the R6G spectrum using a substrate with exposed AuNPs and Figure 4b presents the one using a substrate with buried AuNPs into PMMA. It is possible to identify the characteristic peaks of R6G for both spectra. We also observe that the sample with buried AuNPs presented higher peak intensities and a better signal-to-noise ratio than the sample with exposed AuNPs.

Following this, the effects of AuNP−PMMA substrates annealing on SERS spectra were analyzed. The glass transition temperature (T_G) of PMMA lies between 95 and 106 °C. The temperatures above the T_G allows the mobility of polymer chains around the NPs, leading to the modification of geometric characteristics of metallic NPs.[38] Thus, two substrates of AuNP−PMMA (with buried AuNPs, not exposed) were prepared with a Au implantation dose of 0.81×10^{16} atoms/cm^2 and annealed at 150 °C for 6 h in a hotplate into a laminar flow.[38] Then, the analyte R6G at 10 μM in ethanol was spin-coated over the surface of the substrate.

Figure 5 presents the R6G spectra for the annealed AuNP−PMMA substrate, for the AuNP−PMMA substrate with buried AuNPs, and for the AuNP−PMMA substrate with exposed AuNPs, all with the same ion implantation doses (0.81×10^{16} atoms/cm^2). Additionally, in Figure 5, the R6G spectrum for a bare PMMA substrate (without AuNPs) is shown. In the figure, it is possible to notice the same behavior that was observed in previous results (see Figure 4), where the sample with buried AuNPs presents a better signal than the exposed one. Additionally, it can be noted that the annealed AuNP−PMMA substrate presented the more intense signal, and it is possible to observe that the R6G spectrum of bare PMMA (without AuNPs) does not present any characteristic peak of R6G, as expected.

Concerning the results shown in Figures 4 and 5, we expected to have better signals for the exposed AuNPs and even no significant signal for the buried AuNPs once they are buried 10 nm deep from the surface, that is, there is a too big distance between the R6G analyte and the NPs.

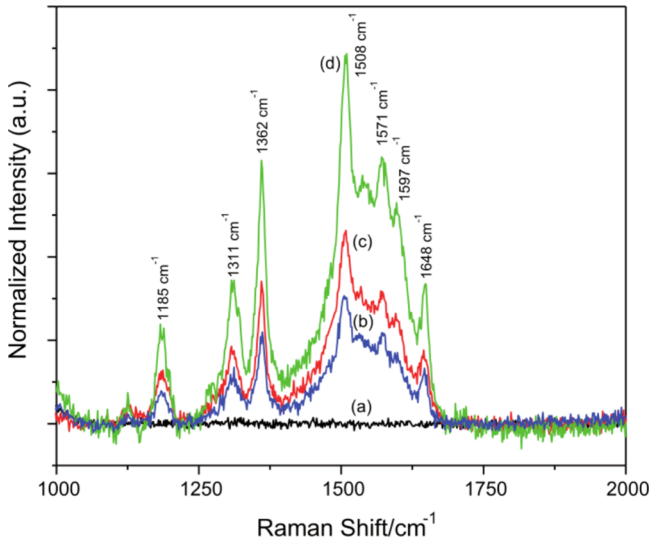

Figure 5. SERS of R6G on (a) PMMA without AuNPs (black); that on (b) exposed AuNPs (blue); that on (c) buried AuNPs (red); and that on (d) annealed buried AuNPs (green). A dose of 0.81×10^{16} atoms/cm^2 for all samples. A baseline correction was applied.

A very reasonable hypothesis that should be considered in the present work is the swelling effect, that is, the increase of a polymer volume when it is immersed in a given solvent. For PMMA, this effect was already studied by Gervinskas and coworkers[39] using solvents such as water, ethanol, and methanol and the swelling occurred for both organic solvents with lower rates for water.

Therefore, because R6G is dissolved in ethanol, the swelling effect seems to favor the entrapment of the R6G molecules in the polymer layer present above and around the NPs, as is the case for buried AuNP−PMMA (annealed and not annealed). Additionally, the study presented by Gervinskas and coworkers[39] describes that coating with gold over PMMA slows the effect of swelling. Thus, in the exposed AuNP−PMMA, the thin layer of exposed AuNPs may be causing the same effect observed in the literature,[39] so that most of R6G molecules remain on the gold layer. In this way, we can propose that the improvement of the SERS signal for the substrates with buried gold below a thin film of PMMA occurs because of a very favorable accumulation of the analyte molecules in the polymer above and around the NPs.

In order to analyze the effect of heating on the AuNP geometry, images by TEM of the composite material AuNP−

https://dx.doi.org/10.1021/acsomega.0c00133
ACS Omega 2020, 5, 10366−10373

PMMA before and after the annealing process were obtained, as is shown in Figure 6. It is notable from the microscopy itself that there is more space between NPs.

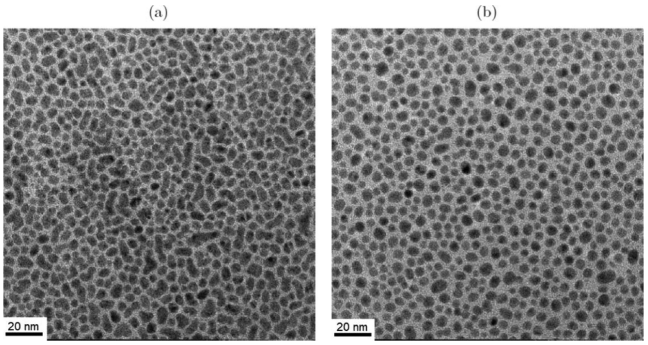

Figure 6. Top-view TEM images of AuNP−PMMA (a) before annealing and (b) after annealing. Dose of implantation: 0.81×10^{16} atoms/cm^2.

Using ImageJ software,[40] it was possible to obtain the particle average diameter and the distance between the particles. The average diameter lies in 5.02 ± 0.03 nm and 5.03 ± 0.02 before and after annealing, respectively, whereas the distance between particles lies in 1.47 ± 0.02 nm and 1.67 ± 0.02 nm before and after annealing, respectively.

Using these parameters, GMM simulations for the SERS EF were performed. Two nanospheres with 5 nm of diameter because the heating process does not significantly alter the AuNPs' dimensions and a separation distance of NPs of 1.5 and 1.6 nm, representing the AuNPs before and after the annealing, respectively, were considered. A dielectric medium containing the NPs also was considered; for this, the choice was water for simplifying the simulations because the proposal of this simulation is to verify the effect of the heating process and consequently the change in the distance between the particles on the SERS signal. The SERS EF was calculated considering the E^4 approximation, which assumes that the EF is proportional to the fourth power of the incident electric field.[41]

According to GMM simulations (Figure 7), there is no increase in the distance between particles that is significant for the improvement of the SERS signal of the annealed sample.

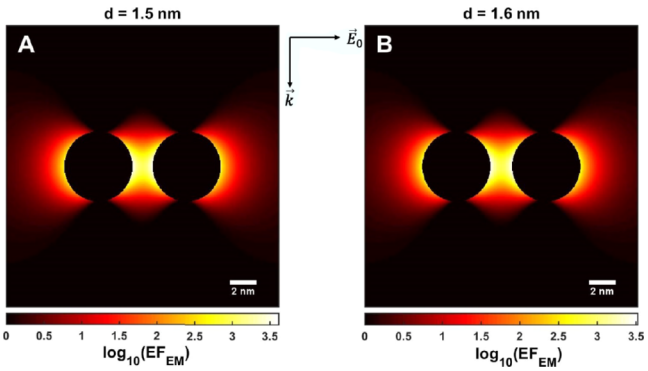

Figure 7. GMM simulation results for the SERS EF of AuNPs (A) before annealing and (B) after annealing, where EF_{EM} refers to the electromagnetic EF because only the electromagnetic intensification of the SERS was considered. The wavelength of incident radiation was considered equal to 633 nm.

Another aspect that should be noted in Figure 6 was the change in the geometry of the NPs after the heating, so that improvement in the uniformity can be observed. For the statistical analysis of the circularity and aspect ratio, a sample of about 8000 NPs of each sample (before and after annealing) was taken, allowing the assembly of a histogram, as is shown in Figure 8.

The histograms were adjusted as a log−normal distribution, with the peaks of distribution related to the most likely values of the circularity and aspect ratio. The formula for circularity is $4\pi(\text{area}/\text{perimeter}^2)$, where a value of 1.0 indicates a perfect circle.[42]

The circularity and the aspect ratio for AuNP−PMMA before annealing lie in 0.89 ± 0.03 and 1.23 ± 0.03, respectively, while for AuNP−PMMA after annealing, the circularity and aspect ratio lie in 0.91 ± 0.02 and 1.17 ± 0.02, respectively. These results indicate that the geometry of AuNPs is predominantly circular for both situations. In addition, the histograms corroborate the fact that the heating process homogenizes the geometry of NPs, a fact that can be verified through the narrowing of the histogram widths because the AuNPs after annealing present a lower variance in their geometries than the AuNPs before annealing. Additionally, it is worth noting that even though the annealing temperature of 150 °C is much lower than the melting temperature of gold, which equals to 1063 °C, the alteration on the geometry of AuNPs occurs because of nanometric scale properties that should be studied further.

The optical properties of the annealed sample were evaluated through UV−vis spectra. For this, the UV−vis spectra for samples consisting of thin films of AuNP−PMMA over glass substrates, with ion implantation doses of 0.60×10^{16} atoms/cm^2, were obtained before and after annealing using the transmission mode for the extinction measurements. The obtained spectra can be seen in Figure 9.

It is possible to notice that there is an expressive increase of the extinction peak and a blue shift of about 70 nm for the sample after annealing. Theoretical calculations described in refs 38 and 43 indicate the possibility of the increase of AuNPs after the annealing process; however, there is no significant increase in the size of the NPs (observed by TEM, Figure 6) which could explain the behavior of the UV−vis spectra. Because the enlargement of the plasmonic band occurs when the electronic densities of the NPs do not oscillate in phase,[44−46] the spectrum of the sample before annealing shows that the presence of NPs of different geometries causes the oscillation of the electronic densities in slightly different frequencies. Thus, the narrowing of the spectrum of the samples after annealing is related to the homogenization of the geometry of the NP, which corroborates with the TEM image analysis.

The roughness of the PMMA surface for bare PMMA (without AuNPs), buried AuNP−PMMA (before and after annealing), and exposed AuNP−PMMA was also evaluated through AFM images, as shown in Table 1.

It is possible to notice that the rms roughness changes significantly only for annealed AuNP−PMMA. Because the SERS spectra for annealed samples showed the best result, it is possible to relate that higher roughness could allow a higher absorption of R6G molecules by the sample surface.[47]

Note that from the gaps between AuNPs determined by TEM images (1.47 ± 0.02 and 1.67 ± 0.02 nm before and after annealing, respectively), we observed, using ImageJ software,

https://dx.doi.org/10.1021/acsomega.0c00133
ACS Omega 2020, 5, 10366−10373

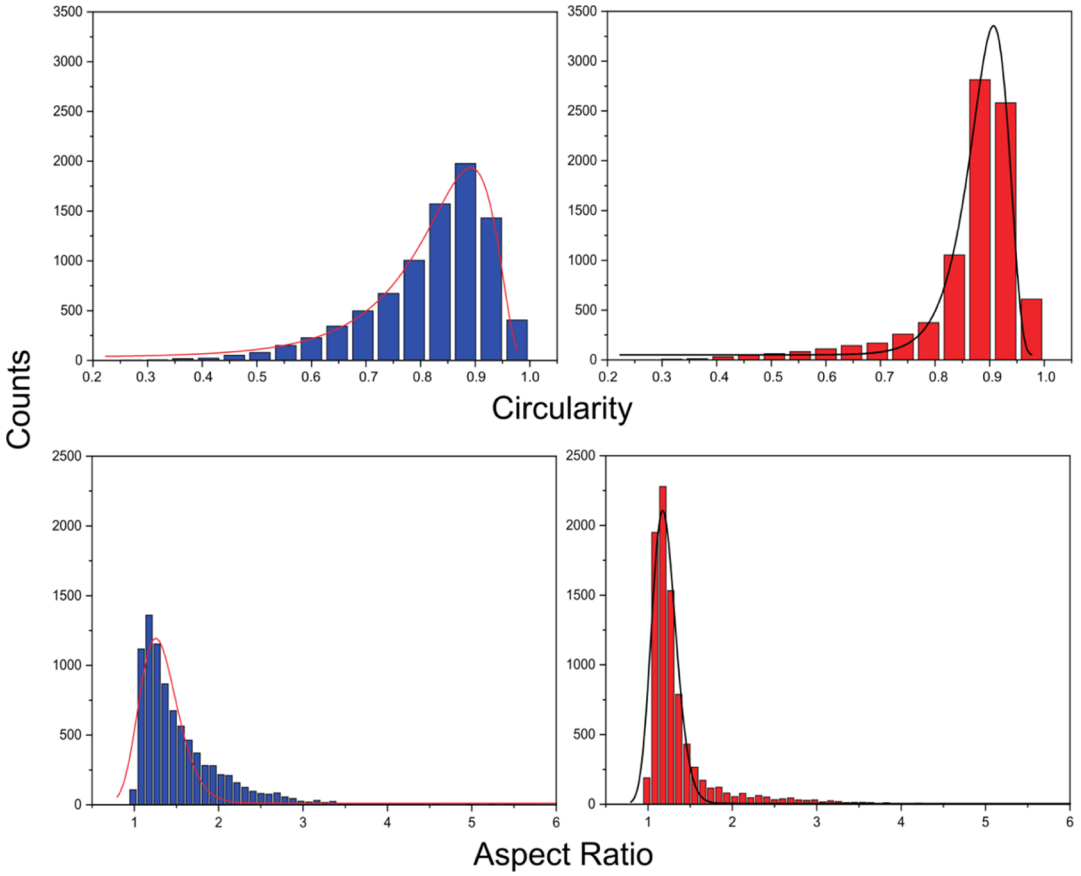

Figure 8. Histograms of the circularity (on the top) and aspect ratio (on the bottom) of AuNP−PMMA before annealing (on the left) and after annealing (on the right).

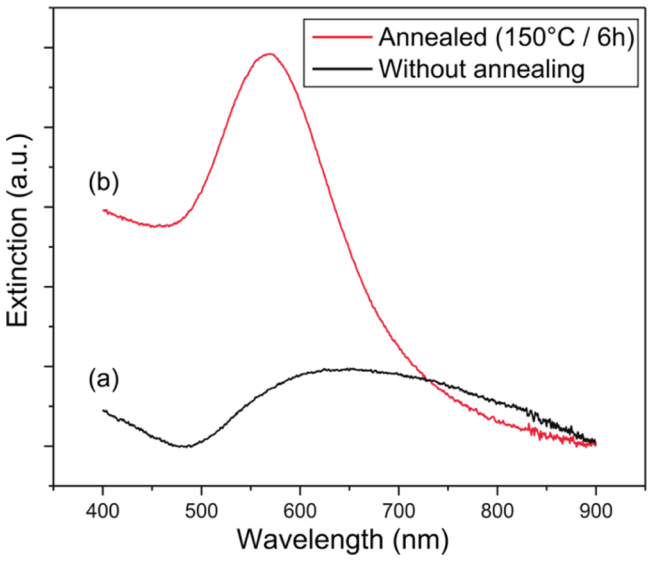

Figure 9. UV−vis spectra of AuNP−PMMA samples (a) before (black) and (b) that after (red) annealing.

that there was an increase of 28% in the polymer area between particles. Considering the swelling and the consequent R6G analyte absorption as the main mechanisms for SERS enhancement, it is in fact clear that intensity of SERS is higher for the annealed samples because there are more R6G molecules near the particles, precisely in the nanogaps, that is, in the hot spot places. This is a very important advance in terms of SERS substrates, overcoming one of the biggest challenges in the area, which is to guide the analyte molecules to the hot spot places.[13]

Table 1. rms Roughness of the PMMA Surface[a]

sample	rms roughness (nm)
bare PMMA	0.61 ± 0.03
exposed AuNP−PMMA	0.61 ± 0.02
buried AuNP−PMMA	0.69 ± 0.01
annealed AuNP−PMMA	1.99 ± 0.01

[a]Ion implantation doses equal to 0.81×10^{16} atoms/cm^2.

CONCLUSIONS

A material composite of gold NPs was formed by low energy ion implantation of gold into a PMMA matrix using a cathodic arc plasma source. The composite layer forms at about 10 nm below the surface of the matrix. The TEM images reveal that the average diameter of the NPs lies between 4.25 and 5.02 nm for different ion implantation doses. Additionally, the TEM image for the annealed sample showed that the heating process homogenizes the NP geometries, a fact that could be demonstrated by statistical analyses. With this material, it was possible to obtain well-resolved SERS spectra of the analyte R6G with a concentration of 10 μM, with the best result for the annealed sample. Additionally, the sample with the buried NPs presented a better SERS spectrum than the exposed ones. This unexpected behavior could be explained by the swelling effect that favors the entrapment of R6G

https://dx.doi.org/10.1021/acsomega.0c00133
ACS Omega 2020, 5, 10366−10373

molecules on the polymer layer above and around the gold NPs. In this context, the annealing also alters the morphological characteristics of the polymer surface, increasing its roughness (and consequently the effective area), favoring the swelling effect. Besides this, the gaps between AuNPs before and after annealing increased 28% in the polymer (projected) area between particles, which traduces in space for more analyte molecules. Thus, the mechanism of improvement of the SERS signal occurs especially because of the higher concentration of R6G molecules around the AuNPs imprisoned on the polymer. Therefore, using absorption of the analyte by PMMA swelling, the molecules are concentrated in the hot spot places between NPs, which consists of an elegant solution to guide molecules to the hot spot places.

AUTHOR INFORMATION

Corresponding Author

Maria Cecilia Salvadori − *Polytechnic School and Institute of Physics, University of São Paulo, CEP 05508-900 São Paulo, São Paulo, Brazil;* orcid.org/0000-0002-2372-1746; Email: mcsalva@if.usp.br

Authors

Natalia K. Gushiken − *Polytechnic School, University of São Paulo, CEP 05508-900 São Paulo, São Paulo, Brazil;* orcid.org/0000-0003-3091-1422

Giordano T. Paganoto − *Institute of Chemistry, University of São Paulo, CEP 05508-000 São Paulo, São Paulo, Brazil*

Marcia L. A. Temperini − *Institute of Chemistry, University of São Paulo, CEP 05508-000 São Paulo, São Paulo, Brazil;* orcid.org/0000-0003-4655-6891

Fernanda S. Teixeira − *Institute of Physics, University of São Paulo, CEP 05315-970 São Paulo, São Paulo, Brazil;* orcid.org/0000-0002-8986-3210

Complete contact information is available at: https://pubs.acs.org/10.1021/acsomega.0c00133

Notes

The authors declare no competing financial interest.

ACKNOWLEDGMENTS

This work was supported by the Conselho Nacional de Desenvolvimento Científico e Tecnológico (CNPq), the Fundação de Amparo a Pesquisa do Estado de São Paulo (FAPESP), the Coordenação de Aperfeiçoamento de Pessoal de Nível Superior (CAPES), and the Financiamento de Estudos e Projetos (Finep), Brazil. The authors are grateful to the team of "Laboratório de Filmes Finos" (LFF) and "Laboratório de Espectroscopia Molecular" (LEM) for assistance in the experimental part and "Centro de Ciência e Tecnologia de Materiais" (CCTM) based in "Instituto de Pesquisas Energéticas e Nucleares" (IPEN) for assistance in obtaining the TEM images. They also thank "Laboratório de Materiais por Feixes Iônicos" (LAMFI) for assistance in RBS analysis.

REFERENCES

(1) Deepak, F. L. *Metal Nanoparticles and Clusters: Advances in Synthesis, Properties and Applications*; Springer, 2017.

(2) Mayer, K. M.; Hafner, J. H. Localized Surface Plasmon Resonance Sensors. *Chem. Rev.* **2011**, *111*, 3828−3857.

(3) Zhang, Y.; Wang, G.; Yang, L.; Wang, F.; Liu, A. Recent Advances in Gold Nanostructures Based Biosensing and Bioimaging. *Coord. Chem. Rev.* **2018**, *370*, 1−21.

(4) Ferreira, J.; Teixeira, F. S.; Zanatta, A. R.; Salvadori, M. C.; Gordon, R.; Oliveira, O. N. Tailored SERS Substrates Obtained with Cathodic Arc Plasma Ion Implantation of Gold Nanoparticles into a Polymer Matrix. *Phys. Chem. Chem. Phys.* **2012**, *14*, 2050−2055.

(5) Uetsuki, K.; Verma, P.; Yano, T.-a.; Saito, Y.; Ichimura, T.; Kawata, S. Experimental Identification of Chemical Effects in Surface Enhanced Raman Scattering of 4-Aminothiophenol. *J. Phys. Chem. C* **2010**, *114*, 7515−7520.

(6) Kerker, M. Electromagnetic Model for Surface-Enhanced Raman Scattering (SERS) on Metal Colloids. *Acc. Chem. Res.* **1984**, *17*, 271−277.

(7) Lombardi, J. R.; Birke, R. L. The Theory of Surface-Enhanced Raman Scattering. *J. Chem. Phys.* **2012**, *136*, 144704.

(8) Zhang, C.; Jiang, S. Z.; Huo, Y. Y.; Liu, A. H.; Xu, S. C.; Liu, X. Y.; Sun, Z. C.; Xu, Y. Y.; Li, Z.; Man, B. Y. SERS Detection of R6G Based on a Novel Graphene Oxide/Silver Nanoparticles/Silicon Pyramid Arrays Structure. *Opt. Express* **2015**, *23*, 24811−24821.

(9) Yu, J.; Guo, Y.; Wang, H.; Su, S.; Zhang, C.; Man, B.; Lei, F. Quasi Optical Cavity of Hierarchical ZnO Nanosheets@Ag Nanoravines with Synergy of Near- and Far-Field Effects for in Situ Raman Detection. *J. Phys. Chem. Lett.* **2019**, *10*, 3676−3680.

(10) Zhang, C.; Li, C.; Yu, J.; Jiang, S.; Xu, S.; Yang, C.; Liu, Y. J.; Gao, X.; Liu, A.; Man, B. SERS Activated Platform with Three-Dimensional Hot Spots and Tunable Nanometer Gap. *Sens. Actuators, B* **2018**, *258*, 163−171.

(11) Li, Z.; Jiang, S.; Huo, Y.; Ning, T.; Liu, A.; Zhang, C.; He, Y.; Wang, M.; Li, C.; Man, B. 3D Silver Nanoparticles with Multilayer Graphene Oxide as a Spacer for Surface Enhanced Raman Spectroscopy Analysis. *Nanoscale* **2018**, *10*, 5897−5905.

(12) Xu, J.; Li, C.; Si, H.; Zhao, X.; Wang, L.; Jiang, S.; Wei, D.; Yu, J.; Xiu, X.; Zhang, C. 3D SERS Substrate Based on Au-Ag Bi-Metal Nanoparticles/MoS2 Hybrid with Pyramid Structure. *Opt. Express* **2018**, *26*, 21546−21557.

(13) Cao, X.; Hong, S.; Jiang, Z.; She, Y.; Wang, S.; Zhang, C.; Li, H.; Jin, F.; Jin, M.; Wang, J. SERS-Active Metal−Organic Frameworks with Embedded Gold Nanoparticles. *Analyst* **2017**, *142*, 2640−2647.

(14) Goul, R.; Das, S.; Liu, Q.; Xin, M.; Lu, R.; Hui, R.; Wu, J. Z. Quantitative Analysis of Surface Enhanced Raman Spectroscopy of Rhodamine 6G Using a Composite Graphene and Plasmonic Au Nanoparticle Substrate. *Carbon* **2017**, *111*, 386−392.

(15) Mishra, Y. K.; Mohapatra, S.; Kabiraj, D.; Mohanta, B.; Lalla, N. P.; Pivin, J. C.; Avasthi, D. K. Synthesis and Characterization of Ag Nanoparticles in Silica Matrix by Atom Beam Sputtering. *Scr. Mater.* **2007**, *56*, 629−632.

(16) Murphy, C. J.; Sau, T. K.; Gole, A. M.; Orendorff, C. J.; Gao, J.; Gou, L.; Hunyadi, S. E.; Li, T. Anisotropic Metal Nanoparticles: Synthesis, Assembly, and Optical Applications. *J. Phys. Chem. B* **2005**, *109*, 13857−13870.

(17) Panáček, A.; Kvítek, L.; Prucek, R.; Kolář, M.; Večeřová, R.; Pizúrová, N.; Sharma, V. K.; Nevěčná, T.; Zbořil, R. Silver Colloid Nanoparticles: Synthesis, Characterization, and Their Antibacterial Activity. *J. Phys. Chem. B* **2006**, *110*, 16248−16253.

(18) Liu, A.; Wang, G.; Wang, F.; Zhang, Y. Gold Nanostructures with Near-Infrared Plasmonic Resonance: Synthesis and Surface Functionalization. *Coord. Chem. Rev.* **2017**, *336*, 28−42.

(19) Tódor, I. S.; Szabó, L.; Marişca, O. T.; Chiş, V.; Leopold, N. Gold Nanoparticle Assemblies of Controllable Size Obtained by Hydroxylamine Reduction at Room Temperature. *J. Nanopart. Res.* **2014**, *16*, 2740.

(20) Guerrini, L.; Garcia-Ramos, J. V.; Domingo, C.; Sanchez-Cortes, S. Sensing Polycyclic Aromatic Hydrocarbons with Dithiocarbamate-Functionalized Ag Nanoparticles by Surface-Enhanced Raman Scattering. *Anal. Chem.* **2009**, *81*, 953−960.

(21) Bell, S. E. J.; Sirimuthu, N. M. S. Quantitative Surface-Enhanced Raman Spectroscopy. *Chem. Soc. Rev.* **2008**, *37*, 1012−1024.

(22) Tan, E.; Yin, P.; Lang, X.; Wang, X.; You, T.; Guo, L. Functionalized Gold Nanoparticles as Nanosensor for Sensitive and Selective Detection of Silver Ions and Silver Nanoparticles by Surface-Enhanced Raman Scattering. *Analyst* **2012**, *137*, 3925−3928.
(23) Kubackova, J.; Fabriciova, G.; Miskovsky, P.; Jancura, D.; Sanchez-Cortes, S. Sensitive Surface-Enhanced Raman Spectroscopy (SERS) Detection of Organochlorine Pesticides by Alkyl Dithiol-Functionalized Metal Nanoparticles-Induced Plasmonic Hot Spots. *Anal. Chem.* **2015**, *87*, 663−669.
(24) Hu, Y.; Liao, J.; Wang, D.; Li, G. Fabrication of Gold Nanoparticle-Embedded Metal−Organic Framework for Highly Sensitive Surface-Enhanced Raman Scattering Detection. *Anal. Chem.* **2014**, *86*, 3955−3963.
(25) Li, J. F.; Huang, Y. F.; Ding, Y.; Yang, Z. L.; Li, S. B.; Zhou, X. S.; Fan, F. R.; Zhang, W.; Zhou, Z. Y.; Wu, D. Y.; Ren, B.; Wang, Z. L.; Tian, Z. Q. Shell-Isolated Nanoparticle-Enhanced Raman Spectroscopy. *Nature* **2010**, *464*, 392−395.
(26) Li, J.-F.; Anema, J. R.; Wandlowski, T.; Tian, Z.-Q. Dielectric Shell Isolated and Graphene Shell Isolated Nanoparticle Enhanced Raman Spectroscopies and Their Applications. *Chem. Soc. Rev.* **2015**, *44*, 8399−8409.
(27) Pham, X.-H.; Hahm, E.; Kim, H.-M.; Shim, S.; Kim, T.; Jeong, D.; Lee, Y.-S.; Jun, B.-H. Silver Nanoparticle-Embedded Thin Silica-Coated Graphene Oxide as an SERS Substrate. *Nanomaterials* **2016**, *6*, 176.
(28) Rao, V. K.; Radhakrishnan, T. P. Tuning the SERS Response with Ag-Au Nanoparticle-Embedded Polymer Thin Film Substrates. *ACS Appl. Mater. Interfaces* **2015**, *7*, 12767−12773.
(29) Stepanov, A. L.; Hole, D. E.; Townsend, P. D. Formation of Silver Nanoparticles in Soda−Lime Silicate Glass by Ion Implantation near Room Temperature. *J. Non-Cryst. Solids* **1999**, *260*, 65−74.
(30) Teixeira, F. S.; Salvadori, M. C. Nucleation of Gold Nanoclusters in PMMA during Energetic Plasma Deposition: A Molecular Dynamics and TfMC-Monte Carlo Study. *Phys. E* **2019**, *112*, 19−25.
(31) Martins, D. R.; Salvadori, M. C.; Verdonck, P.; Brown, I. G. Contamination Due to Memory Effects in Filtered Vacuum Arc Plasma Deposition Systems. *Appl. Phys. Lett.* **2002**, *81*, 1969−1971.
(32) Anders, A.; Yushkov, G. Y. Ion Flux from Vacuum Arc Cathode Spots in the Absence and Presence of a Magnetic Field. *J. Appl. Phys.* **2002**, *91*, 4824−4832.
(33) Salvadori, M. C.; Teixeira, F. S.; Sgubin, L. G.; Cattani, M.; Brown, I. G. Surface Modification by Metal Ion Implantation Forming Metallic Nanoparticles in an Insulating Matrix. *Appl. Surf. Sci.* **2014**, *310*, 158−163.
(34) Salvadori, M. C.; Cattani, M.; Teixeira, F. S.; Brown, I. G. Conducting Polymer Formed by Low Energy Gold Ion Implantation. *Appl. Phys. Lett.* **2008**, *93*, 073102.
(35) Aktary, M.; Stepanova, M.; Dew, S. K. Simulation of the Spatial Distribution and Molecular Weight of Polymethylmethacrylate Fragments in Electron Beam Lithography Exposures. *J. Vac. Sci. Technol., B: Microelectron. Nanometer Struct.–Process., Meas., Phenom.* **2006**, *24*, 768−779.
(36) Wang, M.; Cao, M.; Guo, Z.; Gu, N. Generalized Multiparticle Mie Modeling of Light Scattering by Cells. *Chin. Sci. Bull.* **2013**, *58*, 2663−2666.
(37) Borowicz, P.; Taube, A.; Rzodkiewicz, W.; Latek, M.; Gierałtowska, S. Raman Spectra of High-κ Dielectric Layers Investigated with Micro-Raman Spectroscopy Comparison with Silicon Dioxide. *Sci. World J.* **2013**, *2013*, 1.
(38) Teixeira, F. S.; Salvadori, M. C.; Cattani, M.; Brown, I. G. Annealing Effects on Nanostructured Gold-Polymethylmethacrylate Composites: Small-Angle x-Ray Scattering Analysis. *J. Appl. Phys.* **2012**, *111*, 104311.
(39) Gervinskas, G.; Day, D.; Juodkazis, S. High-Precision Interferometric Monitoring of Polymer Swelling Using a Simple Optofluidic Sensor. *Sens. Actuators, B* **2011**, *159*, 39−43.
(40) Schneider, C. A.; Rasband, W. S.; Eliceiri, K. W. NIH Image to ImageJ: 25 Years of Image Analysis. *Nat. Methods* **2012**, *9*, 671−675.
(41) Le Ru, E. C.; Etchegoin, P. G. Rigorous Justification of Thel El 4 Enhancement Factor in Surface Enhanced Raman Spectroscopy. *Chem. Phys. Lett.* **2006**, *423*, 63−66.
(42) ImageJ Documentation. https://imagej.nih.gov/ij/docs/menus/analyze.html (Accessed date: December 07, 2019).
(43) Li, M.; Cushing, S. K.; Zhang, J.; Lankford, J.; Aguilar, Z. P.; Ma, D.; Wu, N. Shape-Dependent Surface-Enhanced Raman Scattering in Gold−Raman-Probe−Silica Sandwiched Nanoparticles for Biocompatible Applications. *Chem. Soc. Rev.* **2012**, *23*, 115501.
(44) Teixeira, F. S.; Salvadori, M. C.; Cattani, M.; Carneiro, S. M.; Brown, I. G. Surface Plasmon Resonance of Gold Nanoparticles Formed by Cathodic Arc Plasma Ion Implantation into Polymer. *J. Vac. Sci. Technol., B: Microelectron. Nanometer Struct.–Process., Meas., Phenom.* **2009**, *27*, 2242−2247.
(45) Ghosh, S. K.; Pal, T. Interparticle Coupling Effect on the Surface Plasmon Resonance of Gold Nanoparticles: From Theory to Applications. *Chem. Rev.* **2007**, *107*, 4797−4862.
(46) Link, S.; El-Sayed, M. A. Shape and Size Dependence of Radiative, Non-Radiative and Photothermal Properties of Gold Nanocrystals. *Int. Rev. Phys. Chem.* **2000**, *19*, 409−453.
(47) Chatterjee, A.; Gale, D. J. G.; Grebennikov, D.; Whelan, L. D.; Merschrod S, E. F. Surface Potential and Morphology Mapping to Investigate Analyte Adsorption Effects on Surface Enhanced Raman Scattering (SERS). *Chem. Commun.* **2017**, *53*, 12024−12027.

https://dx.doi.org/10.1021/acsomega.0c00133
ACS Omega 2020, 5, 10366−10373